Mineralogical Magazine, October 2016, Vol. 80(6), pp. 1115–1128

Hakite from Příbram, Czech Republic: compositional variability, crystal structure and the role in Se mineralization

P. Škácha[1,2,3,*], J. Sejkora[2], L. Palatinus[4], E. Makovicky[5], J. Plášil[4], I. Macek[2,6] and V. Goliáš[1]

[1] Institute of Geochemistry, Mineralogy and Mineral Resources, Faculty of Science, Charles University in Prague, Albertov 6, CZ–128 43, Prague 2, Czech Republic
[2] Department of Mineralogy and Petrology, National Museum, Cirkusová 1740, Prague 9 - Horní Počernice, 193 00, Czech Republic
[3] Mining muzeum Příbram, Hynka Kličky Place 293, Příbram VI, 261 01
[4] Institute of Physics ASCR, v.v.i., Na Slovance 2, Prague 8, 182 21, Czech Republic
[5] Department of Geosciences and Natural Resource Management, University of Copenhagen, Østervoldgade 10, 1350 Copenhagen K, Denmark
[6] Department of Geological Sciences, Faculty of Science, Masaryk University, Kotlářská 2, 602 00, Brno, Czech Republic

[*Received 10 March 2015; Accepted 12 October 2015; Associate Editor: Marck Welch*]

ABSTRACT

Hakite, ideally $Cu_{10}Hg_2Sb_4Se_{13}$, is a Se-dominant member of the tetrahedrite group occurring at only a few localities in the World. A new occurrence of this mineral in the Příbram uranium and base-metal ore district, Central Bohemia, Czech Republic, is reported in this paper. Hakite was found to be locally abundant and was identified in several samples with Se mineralization. Three chemically distinct types of hakite were distinguished based on electron microprobe study, Hg-rich hakite (hakite *sensu stricto*), Zn-rich hakite and Cd-rich hakite. Hg-hakite dominates among the samples studied. Its average empirical formula based on 29 apfu (n = 54) is $(Cu_{5.61}Ag_{0.39})_{\Sigma 6.00}Cu_{4.00}(Hg_{1.61}Zn_{0.20}Cu_{0.19}Cd_{0.15}Fe_{0.04})_{\Sigma 2.19}$ $(Sb_{3.85}As_{0.28})_{\Sigma 4.13}(Se_{11.55}S_{1.14})_{\Sigma 12.69}$. Less common is the Zn-hakite, $(Cu_{5.80}Ag_{0.20})_{\Sigma 6.00}Cu_{4.00}(Zn_{1.33}Hg_{0.42}Cd_{0.22}Cu_{0.18}Fe_{0.01})_{\Sigma 2.16}(Sb_{3.85}As_{0.26})_{\Sigma 4.11}(Se_{10.92}S_{1.81})_{\Sigma 12.73}$ (n = 22), and rare Cd-hakite has an empirical formula (n = 7) of $(Cu_{5.84}Ag_{0.16})_{\Sigma 6.00}Cu_{4.00}(Cd_{1.27}Zn_{0.60}Cu_{0.10}Hg_{0.07}Fe_{0.02})_{\Sigma 2.06}(Sb_{4.00}As_{0.19})_{\Sigma 4.19}(Se_{12.14}S_{0.61})_{\Sigma 12.75}$. The refined unit cell of Hg-hakite from Příbram, obtained from powder X-ray diffraction data, is a = 10.8783(3) Å with V = 1287.3(1) Å^3 (Z = 4, for the cubic space group $I\bar{4}3m$). Structure refinement from the precession electron diffraction data collected on the transmission electron microscope (R = 24.4% for 424 observed reflections), confirmed that hakite is isostructural with tetrahedrite. The evolution of hydrothermal fluids, from which Se mineralization formed, suggests a distinct enrichment in sulfur and depletion in selenium over the time span of crystallization.

Keywords: hakite, selenides, tetrahedrite group, crystal structure, Příbram, uranium district, analyses, diffraction data.

Introduction

The tetrahedrite group is the most complex isotypic series among the sulfosalts in Nature. This is caused by a multiplicity of iso- and heterovalent substitutions (Möelo *et al.*, 2008). A modern classification of the tetrahedrite group of minerals is lacking. Hakite is a rare Se analogue of tetrahedrite, described for the first time from the Předbořice uranium deposit (Czech Republic, central Bohemia), where it occurs in association with Cu, Pb, Hg and Ag selenides (Johan and Kvaček, 1971). Hakite is, surprisingly, a frequent selenide at the Předbořice deposit, occurring as abundant microscopic grains in carbonate gangue.

*E-mail: skacha-p@muzeum-pribram.cz
DOI: 10.1180/minmag.2016.080.038

© 2016 The Mineralogical Society

https://doi.org/10.1180/minmag.2016.080.038 Published online by Cambridge University Press

Hakite from Předbořice was found to be As- and S-rich (Johan and Kvaček, 1971). Later, the Ag-rich variety of hakite was reported from this locality (Brodin, 1981). Hakite was then described from several other uranium deposits in the Czech Republic (all in western Moravia), such as Bukov (Kvaček, 1973, 1979), Petrovice (Förster *et al.*, 2002) and Rožná – Rozsochy (Kvaček, 1987). The occurrence of the Hg-hakite from Zadní Chodov (Czech Republic, western Bohemia) (Scharmová and Scharm, 1995) is characteristic of a high Se/S ratio of 1/1. A very interesting occurrence of selenide minerals was described by Litochleb *et al*. (1999) from the Ústaleč deposit (Czech Republic, western Bohemia). As-rich hakite and an intermediate member of the giraudite–hakite series were found there as representatives of the tetrahedrite group. Furthermore, (Hg, S)-rich hakite was identified from the small uranium Černý Důl deposit in the Krkonoše Mountains (Kopecký *et al.*, 2010). Microscopic Hg-, Ag- and Cd-hakite was discovered recently at the abandoned Zálesí uranium deposit (Sejkora *et al.*, 2014). Further occurrences are mentioned in the literature from Argentina, Tumiñico (Paar *et al*., 2002) and Germany, Alberoda (Förster *et al.*, 2002; Förster and Rhede, 2004).

The entire uranium and base-metal district of Příbram is situated in exocontact of the Central Bohemian plutonic complex with the Teplá–Barrandien sedimentary unit. Samples containing hakite were collected from the dumps of the uranium shafts No. 16 (Háje) and No. 11A (Bytíz). All the studied polished sections that contain hakite have been deposited in the Mineralogical collection of the National Museum in Prague (Czech Republic). There are four main mineralization stages identified generally in the Příbram uranium and base-metal district: (1) siderite-sulfidic; (2) calcite; (3) calcite-uraninite; (4) calcite-sulfidic. Selenide mineralization occurs usually in close association with uraninite during the calcite-uraninite mineralization stage. Uranium ore is represented by uraninite, coffinite and U-bearing antraxolite. The age of the uranium mineralization obtained by U-Pb radiometric age determination of uraninite is middle Permian, 275 ± 4 and 278 ± 4 Ma (Anderson, 1987). According to a fluid inclusion study (Žák and Dobeš, 1991), the carbonate veins carrying uraninite in the Příbram district, formed at low temperatures (80–140°C) and at low salinities. Selenides in carbonate veins follow the crystallization of uraninite, as is observed in other hydrothermal vein uranium deposits (Dymkov, 1985).

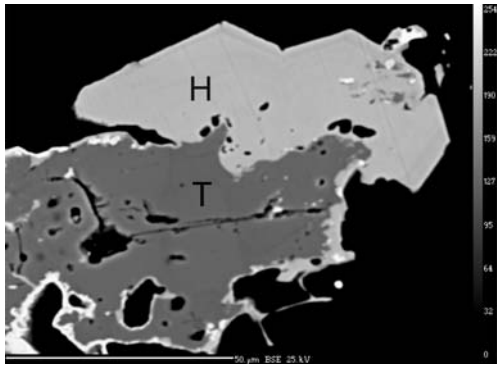


FIG. 1. Perfectly developed hakite (H) crystal growing on Se-tetrahedrite (T), probably the result of the younger hydrothermal remobilization processes.

Occurrence and sample descriptions

In the samples studied hakite usually forms abundant grains up to 2 mm in size and their aggregates up to 5 mm across, growing in calcite, or forms an intergrowth with other sulfides and selenides. Exceptionally in a single specimen, a euhedral crystal of hakite occurred, as shown in Fig. 1. Hakite from Příbram is metallic grey with a brownish tint; it associates closely with other selenides, sulfides and ubiquitous uraninite; it encloses clausthalite, tiemannite and eskebornite, and is enclosed in turn by tetrahedrite and eskebornite. Aggregates of hakite, sometimes accompanied by clausthalite, are overgrown by Se-rich tetrahedrite. Compositional zonation in hakite aggregates, caused by repeating cycles of hakite and Se-tetrahedrite crystallization, was observed only rarely (Fig. 2). The general crystallization sequence, deduced from a large number of samples, can be represented as uraninite → clausthalite + tiemannite → eskebornite → hakite → Se-tetrahedrite → tetrahedrite + chalcopyrite. The most important minerals and mineral associations relevant to the genesis of hakite at Příbram are summarized in Table 1.

Composition

The composition of the hakite samples studied was obtained using a Cameca SX100 electron microprobe (National Museum, Prague) operating in wavelength-dispersive mode (WDS) using 25 kV and 20 nA, and

https://doi.org/10.1180/minmag.2016.080.038 Published online by Cambridge University Press

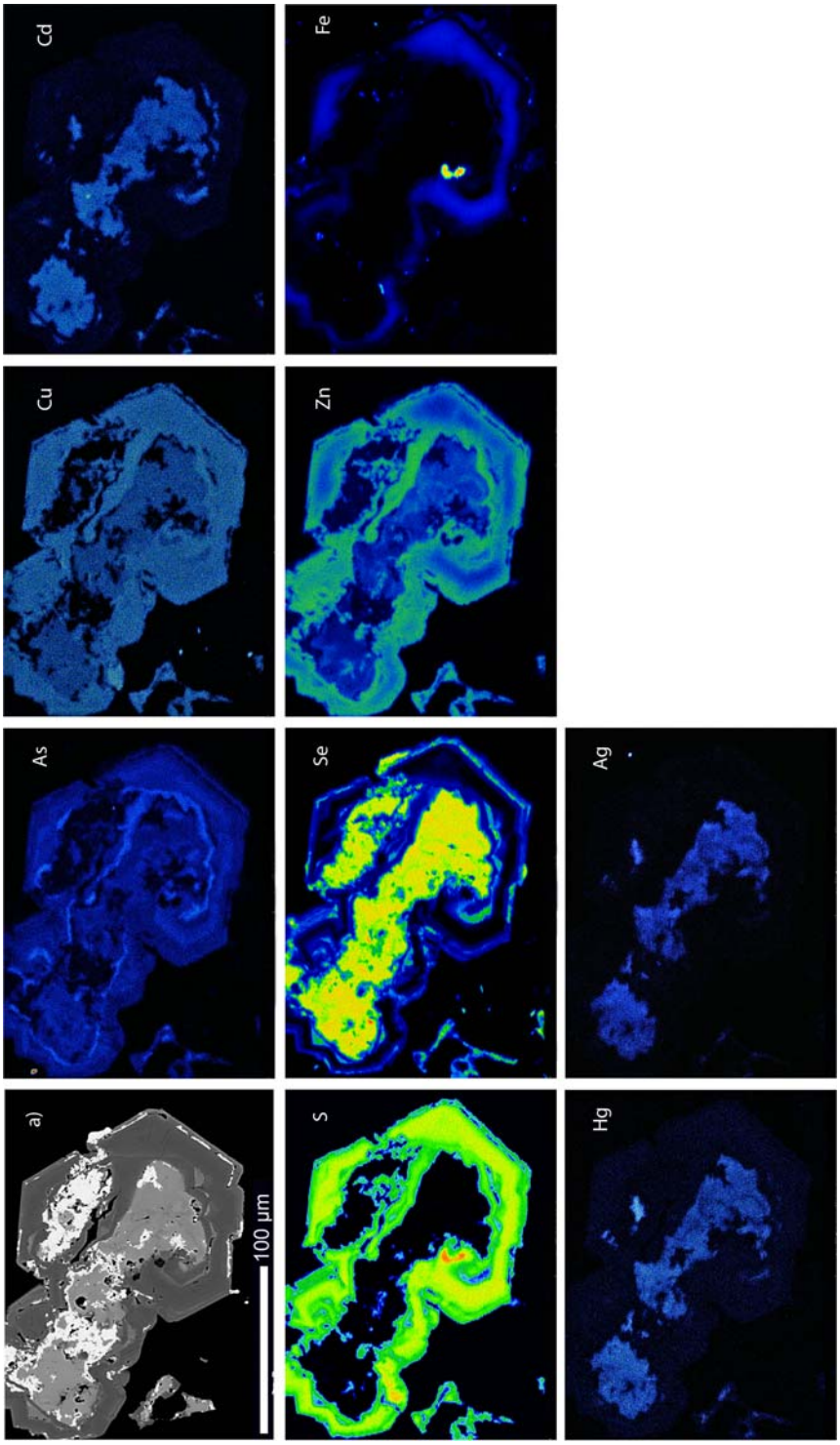


FIG. 2. Back-scattered electron image (*a*) and X-ray element distribution maps for As, S, Se, Hg, Ag, Cu, Cd, Zn and Fe showing the internal zoning within the composite crystal aggregate of tetrahedrite-Se (dark grey) – hakite (light grey) with clausthalite inclusions (white). The Fe and S anomaly in tetrahedrite-Se probably belongs to pyrite. An As anomaly outside the hakite-tetrahedrite-Se crystal aggregate belongs to an undefined recent As mineral.

https://doi.org/10.1180/minmag.2016.080.038 Published online by Cambridge University Press

TABLE 1. The most important minerals associated with hakite at Příbram.

Mineral	Ideal composition	Associated minerals	Textural associations
Antimonselite	Sb_2Se_3	Hg-hakite, Se-chalcostibite	euhedral crystals up to 1.5 mm
Athabascaite	Cu_5Se_4	Hg-hakite	anhedral grains up to 300 μm
Berzelianite	Cu_7Se_4	Hg-hakite, Zn-hakite, umangite	anhedral grains up to 2 mm
Bukovite	$Tl_2(Cu,Fe)_4Se_4$	Zn-hakite, umangite, eucairite	idiomorphic grains up to 30 μm
Cadmoselite	CdSe	Cd-hakite, clausthalite	anhedral and euhedral grains up to 40 μm
Chalcopyrite	$CuFeS_2$	Tetrahedrite	anhedral and euhedral grains up to 10 mm
Clausthalite	PbSe	Hg-hakite, Cd-hakite, tetrahedrite	anhedral and euhedral grains up to 2 mm
Dzharkenite	FeSe	Hg-hakite, tiemannite, tetrahedrite	euhedral and subhedral crystals up to 60 μm
Eskebornite	$CuFeSe_2$	Zn-hakite, Hg-hakite, umangite	anhedral grains up to 2 mm
Giraudite	$Cu_6[Cu_4(Fe,Zn)_2]As_4Se_{13}$	Zn-hakite, berzelianite	anhedral grains and rims up to 30 μm
Se-analogue of chalcostibite	$CuSbSe_2$	Hg-hakite, dzharkenite, tiemannite	euhedral crystals up to 10 μm
Löllingite	$FeAs_2$	Hg-hakite, clausthalite	anhedral grains up to 30 μm
Tetrahedrite	$Cu_6[Cu_4(Fe,Zn)_2]Sb_4Se_{13}$	Chalcopyrite, Hg-hakite	anhedral and euhedral grains up to 10 mm
Tiemannite	HgSe	Hg-hakite, antimonselite	anhedral grains up to 2 mm
Umangite	Cu_3Se_2	Berzelianite, Hg-hakite	anhedral grains up to 3 mm

a beam diameter of ~1 μm. The following standards and X-ray lines were used to minimize line overlaps: Ag (Ag*L*α), Au (Au*M*α), Bi (Bi*M*β), CdTe (Cd*L*α), Co (Co*K*α), chalcopyrite (Cu*K*α), FeS_2 (Fe*K*α, S*K*α), HgTe (Hg*M*α), NiAs (Ni*K*α, As*L*α), PbS (Pb*M*α), PbSe (Se*L*α), PbTe (Te*L*α), Sb_2S_3 (Sb*L*α), Tl (Br,I) (Tl*L*α) and ZnS (Zn*K*α). Peak counting times were 20 s for all elements, and one half of the peak time for each background. Gold, Bi, Co and Ni were below detection limits (0.02–0.05 wt.%). Raw intensities were converted to the concentrations of elements using automatic *PAP* (Pouchou and Pichoir, 1985) matrix-correction software. All tetrahedrite-group analyses, including plots, are based on 29 atoms per formula unit (apfu).

Minerals of the tetrahedrite group are well known to have extensive substitutional possibilities. A general formula for minerals of the tetrahedrite group can be expressed according to Moëlo *et al.* (2008) as $^{[III]}A_6{}^{[IV]}(B,C)_6{}^{[III]}X_4{}^{[IV]}Y_{12}{}^{[VI]}Z_1$, where A = Cu, Ag; B = Cu^{1+}, Ag, and C is generally a divalent metal (typically Fe, Zn, but also Hg, Mn, Cd, Cu^{2+} etc.) in the same coordination as B; X = Sb, As, Bi, Te; Y and Z = S and Se. Even though the C site is not an individual site and has the same character as the B site, the tetrahedrite group of minerals is classified in the literature by not only the Sb/As ratio, but also according to the content of divalent metal. For this case it is possible to apply the dominant-constituent rule (Hatert and Burke, 2008). Hakite was described originally as a Hg variety, but for the matter of classification we propose to apply the 50% rule (on the atomic basis) for solid solutions of the selenium members of the tetrahedrite group. For this reason the following text distinguishes Zn-, Cd- and also Hg-hakite.

The tetrahedrite/hakite composite aggregate found in one of the samples (Fig. 2) shows an unusual variability in the chemical composition. Interpreting these compositional trends we can assume implications for the mineralization sequence in the deposit. Representative results of the electron-microprobe analyses of this composite crystal aggregate are given in Table 2. Selected results of the electron microprobe analyses of Hg-hakite, Zn-hakite and Cd-hakite from various samples from Příbram are given in Table 3. In the analysed samples, copper predominates at the A site. The Hg-hakite contains up to 1.2 apfu Ag, which is more than observed in Zn- and Cd-hakites (Fig. 3). Coexisting tetrahedrite has very minor Ag contents. The average Ag content in the Hg-hakite is 0.39 apfu (n = 54) and in the Zn-hakite and the Cd-hakite it is 0.20 (n = 22) and 0.16 (n = 7) Ag apfu, respectively. The B position is fully occupied

https://doi.org/10.1180/minmag.2016.080.038 Published online by Cambridge University Press

https://doi.org/10.1180/minmag.2016.080.038 Published online by Cambridge University Press

TABLE 2. Representative analyses of the minerals of the tetrahedrite group from the composite aggregate in Fig. 2.*

Analysis No.	1	2	3	4	5	6	7	8	9	10	11	12	13	14	15
Cu	38.47	36.92	37.37	37.24	34.51	26.01	23.41	23.04	25.38	22.09	22.77	27.38	26.72	26.66	26.38
Ag	0.10	0.04	0.03	0.06	0.07	1.85	4.48	3.85	1.55	4.06	4.36	1.19	1.10	1.21	1.27
Hg	0.00	0.03	0.03	0.07	0.03	7.41	12.39	12.18	6.93	11.90	12.23	4.53	5.24	4.48	4.67
Zn	3.98	5.50	3.71	4.04	6.47	1.60	0.17	0.13	1.57	0.09	0.12	3.16	2.25	2.70	2.67
Fe	3.34	1.32	3.14	2.85	0.25	0.00	0.13	0.08	0.01	0.05	0.04	0.00	0.02	0.01	0.01
Pb	0.00	0.03	0.10	0.08	0.60	0.00	0.00	0.00	0.17	0.00	0.00	0.00	0.00	0.00	0.00
Cd	0.43	0.28	0.30	0.34	0.04	2.80	1.82	1.61	2.75	1.72	1.70	2.17	2.64	2.09	2.13
Sb	28.59	27.18	27.94	27.64	25.50	20.32	17.22	11.84	18.93	15.78	16.41	21.42	20.46	19.46	20.20
As	0.76	2.16	2.25	2.47	2.86	0.27	1.74	5.14	1.30	3.38	2.86	0.22	1.20	1.69	1.13
Se	1.68	4.39	2.65	1.42	9.02	38.16	37.42	40.34	39.10	40.02	39.47	36.95	37.02	39.07	39.85
S	24.38	21.95	23.65	24.29	19.10	1.11	0.60	0.72	1.54	0.70	0.63	2.13	3.07	2.15	1.62
total	101.73	99.80	101.16	100.50	98.45	99.54	99.37	98.93	99.22	99.78	100.61	99.15	99.73	99.52	99.93
Cu_{TOT}	9.986	10.002	9.824	9.774	9.790	9.881	9.283	8.936	9.536	8.642	8.871	10.034	9.644	9.671	9.658
Cu	9.985	9.993	9.824	9.774	9.790	9.587	8.954	8.936	9.536	8.642	8.871	9.742	9.644	9.671	9.658
Ag	0.015	0.007	0.004	0.010	0.012	0.413	1.046	0.880	0.342	0.936	1.001	0.258	0.235	0.258	0.274
Sum M^{+}	10.000	10.000	9.828	9.783	9.802	10.000	10.000	9.815	9.878	9.578	9.872	10.000	9.878	9.929	9.932
Cu**	0.000	0.009	0.000	0.000	0.000	0.294	0.329	0.000	0.000	0.000	0.000	0.292	0.000	0.000	0.000
Hg	0.000	0.002	0.002	0.006	0.002	0.892	1.557	1.496	0.824	1.474	1.510	0.526	0.599	0.515	0.542
Zn	1.005	1.447	0.949	1.032	1.784	0.592	0.064	0.050	0.575	0.035	0.046	1.125	0.790	0.952	0.951
Fe	0.985	0.407	0.938	0.852	0.081	0.000	0.058	0.036	0.004	0.022	0.018	0.000	0.006	0.004	0.003
Pb	0.000	0.002	0.008	0.006	0.053	0.000	0.000	0.000	0.020	0.000	0.000	0.000	0.000	0.000	0.000
Cd	0.063	0.043	0.045	0.050	0.007	0.602	0.407	0.354	0.584	0.379	0.375	0.449	0.540	0.429	0.440
Sum M^{2+}	2.054	1.910	1.942	1.945	1.927	2.380	2.415	1.936	2.006	1.911	1.948	2.393	1.936	1.900	1.937
Sb	3.873	3.844	3.833	3.786	3.776	4.028	3.563	2.397	3.712	3.222	3.337	4.097	3.855	3.685	3.861
As	0.167	0.497	0.501	0.550	0.688	0.088	0.586	1.689	0.414	1.120	0.946	0.068	0.369	0.520	0.352
Sum X^{3+}	4.040	4.341	4.334	4.336	4.465	4.117	4.150	4.086	4.126	4.342	4.283	4.165	4.223	4.205	4.213
Se	0.351	0.956	0.561	0.300	2.059	11.667	11.942	12.591	11.824	12.597	12.374	10.898	10.755	11.406	11.742
S	12.541	11.786	12.324	12.633	10.739	0.836	0.475	0.551	1.145	0.544	0.485	1.545	2.197	1.549	1.173
Sum $(Y+Z)^{2-}$	12.891	12.742	12.885	12.933	12.798	12.503	12.417	13.143	12.969	13.142	12.859	12.442	12.952	12.955	12.915

*The number of atoms is normalized to 29 apfu. **Cu calculated as $Cu_{tot} - (10 - Ag_{tot})$. Analyses 1–5 are for Zn-tetrahedrite, 6–11 for Hg-hakite, 12–15 for Zn-hakite.

https://doi.org/10.1180/minmag.2016.080.038 Published online by Cambridge University Press

TABLE 3. Representative analyses of Hg, Zn and Cd-hakite from various samples from Příbram.

	Mean 1	1	2	3	4	Mean 2	5	6	7	8	Mean 3	9	10	11	12
Cu	25.32	28.54	23.41	24.32	25.62	27.97	27.73	29.39	31.38	26.67	27.25	27.14	26.74	27.45	27.06
Ag	1.70	0.28	4.48	0.75	1.19	0.94	1.67	0.14	0.21	2.10	0.76	0.73	0.60	0.92	0.71
Hg	13.15	12.50	12.39	15.25	13.51	3.69	4.02	1.99	3.65	4.20	0.64	0.64	0.12	1.25	0.57
Zn	0.52	1.10	0.17	0.00	0.61	3.83	4.18	5.31	4.71	3.75	1.69	1.49	2.53	1.23	1.54
Fe	0.10	0.00	0.13	0.13	0.08	0.03	0.11	0.00	0.07	0.16	0.04	0.06	0.07	0.13	0.00
Pb	0.03	0.00	0.00	0.00	0.00	0.00	0.00	0.00	0.00	0.00	0.03	0.08	0.00	0.00	0.10
Cd	0.67	0.28	1.82	0.00	0.19	1.11	0.30	0.00	0.20	0.41	6.14	6.55	5.17	6.55	6.26
Sb	19.04	20.87	17.22	19.20	19.77	20.68	19.00	21.62	22.10	19.32	21.02	21.22	21.26	21.34	21.29
As	0.84	0.17	1.74	0.36	0.08	0.85	1.50	0.23	0.29	1.43	0.62	0.51	0.23	0.48	0.44
Se	37.09	32.54	37.42	38.55	38.33	38.04	41.13	39.79	30.38	40.87	41.36	41.62	39.89	41.04	41.58
S	1.49	4.32	0.60	0.76	0.33	2.56	1.04	1.80	6.43	0.70	0.84	0.54	2.27	0.75	0.56
Total	99.94	100.60	99.37	99.31	99.71	99.73	100.68	100.27	99.43	99.60	100.40	100.59	98.87	101.13	100.10
Cu_{TOT}	9.798	10.39	9.289	9.715	10.137	9.978	9.964	10.351	10.531	9.806	9.937	9.950	9.630	10.020	9.960
Cu	9.613	9.940	8.953	9.715	9.724	9.803	9.648	9.971	9.959	9.545	9.836	9.842	9.630	9.800	9.850
Ag	0.387	0.060	1.047	0.176	0.276	0.197	0.352	0.029	0.041	0.455	0.164	0.158	0.130	0.200	0.150
Sum M^{+}	10.000	10.000	10.000	9.891	10.000	10.000	10.000	10.000	10.000	10.000	10.000	10.000	9.760	10.000	10.000
Cu**	0.185	0.447	0.336	0.000	0.414	0.175	0.317	0.380	0.572	0.260	0.100	0.109	0.000	0.220	0.110
Hg	1.612	1.441	1.558	1.930	1.694	0.417	0.458	0.222	0.388	0.490	0.074	0.075	0.010	0.140	0.070
Zn	0.197	0.389	0.064	0.000	0.234	1.329	1.462	1.817	1.537	1.342	0.599	0.531	0.890	0.440	0.550
Fe	0.043	0.000	0.058	0.059	0.035	0.013	0.044	0.000	0.027	0.066	0.018	0.025	0.030	0.050	0.000
Pb	0.003	0.000	0.000	0.000	0.000	0.000	0.000	0.000	0.000	0.000	0.003	0.009	0.000	0.000	0.010
Cd	0.147	0.058	0.408	0.000	0.043	0.225	0.061	0.000	0.038	0.084	1.266	1.357	1.050	1.350	1.300
Sum M^{2+}	2.188	2.336	2.423	1.989	2.420	2.159	2.342	2.419	2.562	2.242	2.060	2.106	1.980	2.200	2.040
Sb	3.846	3.964	3.566	4.003	4.083	3.851	3.564	3.974	3.872	3.708	4.001	4.061	4.000	4.060	4.090
As	0.276	0.052	0.587	0.122	0.027	0.258	0.457	0.068	0.083	0.447	0.191	0.160	0.070	0.150	0.140
Sum X^{3+}	4.122	4.017	4.152	4.125	4.111	4.109	4.021	4.043	3.954	4.155	4.192	4.220	4.070	4.210	4.230
Se	11.550	9.531	11.950	12.392	12.209	10.920	11.894	11.279	8.205	12.096	12.137	12.280	11.570	12.050	12.320
S	1.139	3.116	0.475	0.603	0.261	1.811	0.744	1.259	4.278	0.507	0.610	0.394	1.620	0.540	0.410
Sum $(Y+Z)^{2-}$	12.690	12.647	12.425	12.995	12.470	12.732	12.637	12.538	12.483	12.603	12.747	12.674	13.190	12.590	12.730

*The number of ions is normalized to 29 apfu. **Cu calculated as $Cu_{tot} - (10–Ag_{tot})$; mean 1 and 1–4: average of all 54 analyses of Hg-hakite and its representative analyses; mean 2 and 5–8: average of all 22 analyses of Zn-hakite and its representative analyses; mean 3 and 9–12: average of all seven analyses of Cd-hakite and its representative analyses.

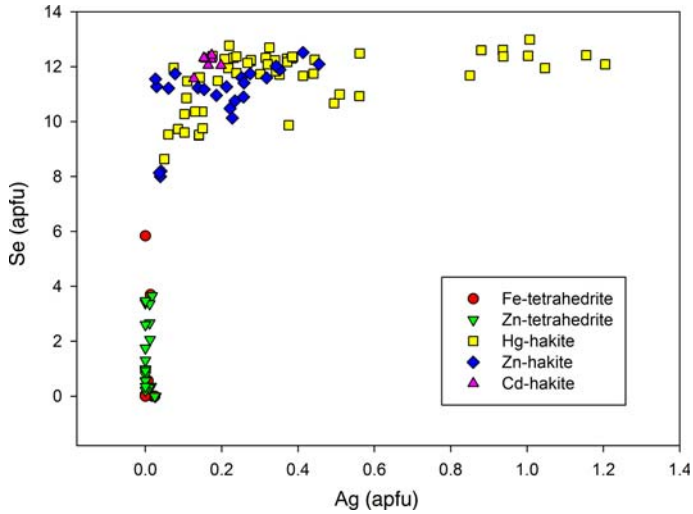


FIG. 3. Plot of Ag and Se contents (apfu) for the investigated hakite and tetrahedrite from Příbram. Preferential ordering of Ag at the A site in hakite is evident.

by copper in all the samples analysed. Dominant iron and zinc is typical for the *C* site in tetrahedrite. However, prevailing mercury, and less frequently zinc, copper and cadmium are typical for analysed hakite at the *C* site (Fig. 4). Antimony is dominant over arsenic at the *X* site, (Fig. 5). Selenium or sulfur end-members of the hakite–tetrahedrite series were analysed as well as the intermediate members (Fig. 6). In the samples studied Hg-hakite dominates. On the basis of 54 WDS analyses, its empirical formula based on 29 apfu is $(Cu_{5.61}Ag_{0.39})_{\Sigma 6.00}Cu_{4.00}(Hg_{1.61}Zn_{0.20}Cu_{0.19}Cd_{0.15}Fe_{0.04})_{\Sigma 2.19}(Sb_{3.85}As_{0.28})_{\Sigma 4.13}(Se_{11.55}S_{1.14})_{\Sigma 12.69}$. The empirical formula of the Zn-hakite (n = 22) is $(Cu_{5.80}Ag_{0.20})_{\Sigma 6.00}Cu_{4.00}(Zn_{1.33}Hg_{0.42}Cd_{0.22}Cu_{0.18}Fe_{0.01})_{\Sigma 2.16}(Sb_{3.85}As_{0.26})_{\Sigma 4.11}(Se_{10.92}S_{1.81})_{\Sigma 12.73}$, and for the Cd-hakite $(Cu_{5.84}Ag_{0.16})_{\Sigma 6.00}Cu_{4.00}(Cd_{1.27}Zn_{0.60}Cu_{0.10}Hg_{0.07}Fe_{0.02})_{\Sigma 2.06}(Sb_{4.00}As_{0.19})_{\Sigma 4.19}(Se_{12.14}S_{0.61})_{\Sigma 12.75}$ (n = 7).

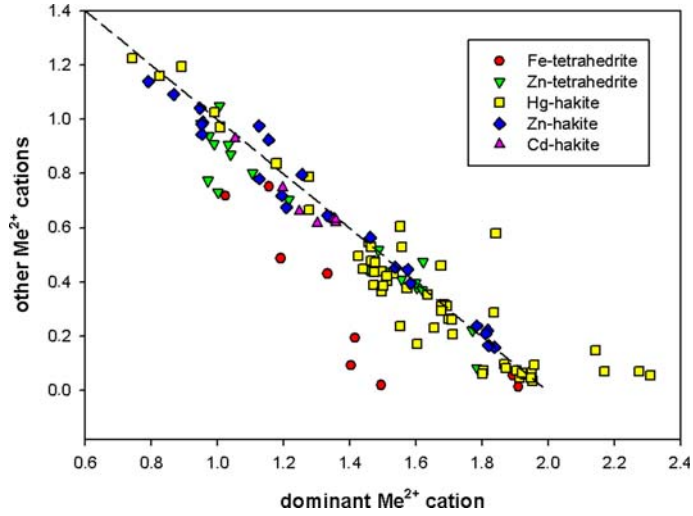


FIG. 4. Plot of dominant Me^{2+} cation and other Me^{2+} cations in the *C* position for the individual hakite and tetrahedrite types from Příbram. The line is for C = 2 apfu.

https://doi.org/10.1180/minmag.2016.080.038 Published online by Cambridge University Press

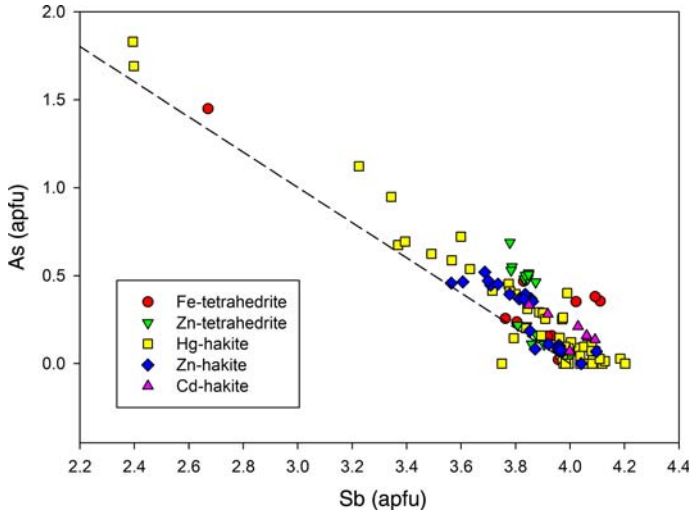


FIG. 5. Plot of Sb and As contents (apfu) of Cd, Zn and Hg-hakite and Zn and Fe-tetrahedrite from Příbram. The line is for $X = 4$ apfu.

Powder X-ray diffraction

A powder X-ray diffraction pattern of Hg-hakite (Table 3, analysis 1) was obtained from a hand-picked pulverized sample using a Bruker D8 Advance diffractometer (National Museum, Prague) equipped with the solid-state 1D LynxEye detector (Cu$K\alpha$ radiation, 40 kV, 40 mA). In order to minimize an elevated background, the pulverized sample was placed on the surface of a flat silicon wafer using an acetone suspension. Powder data were collected in Bragg–Brentano geometry in the range of 4–75°2θ, a step interval of 0.01° and a counting time of 30 s per step. Pure silicon was used as an external standard. Positions and intensities of reflections were found and refined using the PearsonVII profile-shape function employing the *ZDS* program package (Ondruš, 1995). Unit-cell

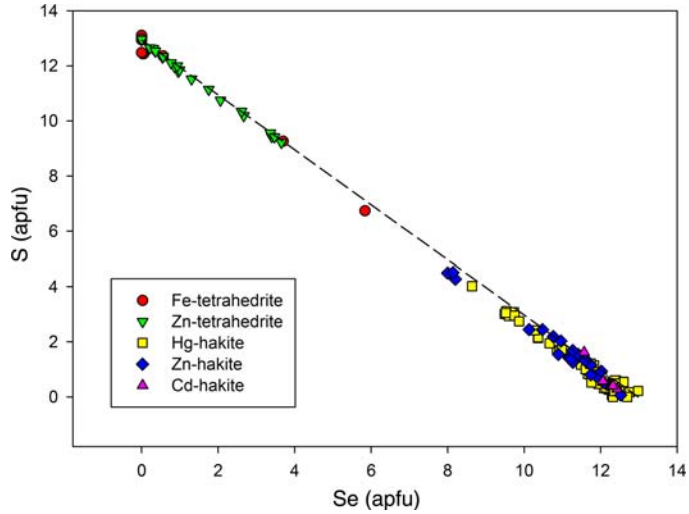


FIG. 6. Plot of Se and S contents (apfu) of Cd, Zn and Hg-hakite and Zn and Fe-tetrahedrite from Příbram. The line is for $Z = 13$ apfu.

https://doi.org/10.1180/minmag.2016.080.038 Published online by Cambridge University Press

TABLE 4. Powder X-ray diffraction data (Å) for hakite from Příbram.

h	*k*	*l*	d_{obs}	d_{calc}	I_{rel}	I_{calc}*
1	1	0	7.695	7.692	2	<1
2	0	0	5.438	5.439	1	<1
2	1	1	4.441	4.441	5	5
2	2	0	3.846	3.846	4	8
3	1	0	3.441	3.440	1	5
2	2	2	3.140	3.140	100	100
3	2	1	2.908	2.907	8	20
4	0	0	2.719	2.720	8	8
4	1	1	2.564	2.564	7	14
3	3	0	2.564	2.564	7	4
4	2	0	2.4327	2.4325	1	3
3	3	2	2.3197	2.3193	1	4
4	2	2	2.2203	2.2205	1	3
4	3	1	2.1333	2.1334	4	11
5	2	1	1.9859	1.9861	7	18
4	4	0	1.9226	1.9230	26	55
4	3	3	1.8651	1.8656	3	6.1
4	4	2	1.8133	1.8131	<1	1
6	1	1	1.7644	1.7647	3	19
6	2	0	1.7198	1.7200	1	50
6	2	2	1.6403	1.6400	10	21
6	3	1	1.6035	1.6039	<1	1
4	4	4	1.5701	1.5702	1	2
5	4	3	1.5386	1.5384	1	4
5	5	0	1.5386	1.5384	1	4
6	3	3	1.4806	1.4804	1	1
5	5	2	1.4806	1.4804	1	1
8	0	0	1.3596	1.3598	1	5
7	4	1	1.3389	1.3390	1	3
6	5	3	1.3004	1.3002	1	11

*Calculated (Yvon *et al.*, 1977) from crystal structure information of hakite (this study).

parameters were refined by the least-squares program of Burnham (1962). Powder X-ray diffraction data of the Hg-hakite from Příbram are given in Table 4 along with comparison of Hg-hakite data from the Předbořice locality (Johan and Kvaček, 1971). Refinement of the unit cell of the Hg-hakite (space group $I\bar{4}3m$) gave $a = 10.8783(3)$ Å, with $V = 1287.3(1)$ Å^3, consistent with published data for Hg-hakite from Předbořice (Table 5). Shannon's (1981) radii for sulfides are for Hg^{2+} (in tetrahedral coordination) 0.84 Å, for S^{2-} 1.70 Å and Se^{2-} 1.84 Å, so that model Hg–X distances in HgX_4 tetrahedra are 2.54 and 2.68 Å for S and Se, respectively. The bonds in tetrahedra in the structures of the tetrahedrite group of minerals are oriented along body diagonals of the cubic unit cell.

TABLE 5. Unit-cell parameters of hakite ($I\bar{4}3m$).

Locality	Type	*a* [Å]	*V* [Å^3]	Reference
Příbram	Hg	10.8783(3)	1287.3(1)	This study
Předbořice	Hg	10.88(1)	1287.9(4)	Johan and Kvaček (1971)
Předbořice	Ag	10.40	1124.9	Brodin (1981)

Therefore, when based on the unit-cell parameter of $Cu_{10}Hg_2Sb_4S_{13}$ (10.515 Å; Karup-Møller and Makovicky, 2003), this calculation results in 10.850 Å, in reasonable agreement with the value obtained for studied hakite of 10.878 Å.

Transmission electron microscopy

A small amount of Hg-hakite was ground under ethanol in an agate mortar and a suspension was deposited onto a TEM grid (Cu grid with carbon coating). A well-diffracting crystal in the form of an approximate equilateral triangle with an edge of 0.7 μm was selected for the data acquisition. Data were collected employing the electron diffraction tomography method (Kolb *et al.*, 2007). The crystal was tilted by 1° step intervals around the goniometer axis in the range –58° to 50°, giving a total of 109 diffraction patterns. Diffraction patterns were processed using the *PETS* program (Palatinus, 2011) and *Jana2006* (Petříček *et al.*, 2014) to obtain the unit cell, orientation matrix and integrated reflection intensities. The single-crystal XRD study was not realized due to the highly zoned nature of the seldom-observed crystals. We note that, in general, unit-cell parameters obtained from PED (precession electron diffraction) are inherently less accurate than those obtained from powder diffraction. Therefore in all refinements and subsequent calculations involving PED data, the cell parameters obtained from the powder diffraction were used.

Using the intensity data from electron diffraction, the crystal structure of hakite was solved *ab initio* by the charge-flipping algorithm of the *Superflip* program (Palatinus and Chapuis, 2007) and refined subsequently by *Jana2006* (Petříček *et al.*, 2014) based on *F*. The approximation that the integrated intensities are proportional to $|F|^2$ was used in the refinement. This is only a very rough approximation for the electron diffraction data and so the resulting structural parameters must be treated as being only approximate. Diffraction patterns of the

https://doi.org/10.1180/minmag.2016.080.038 Published online by Cambridge University Press

TABLE 6. Data collection and refinement characteristics for the structure solution and refinement of Hg-hakite.

Chemical formula	$Cu_{10.77}Hg_{1.22}Sb_4Se_{13}$
M	2441.9
Crystal system	Cubic,
Space group	$I\bar{4}3m$
Temperature (K)	293
a (Å)	11.2802
V (Å^3)	1435.33
Z	2
Radiation type	Electron, λ = 0.0335 Å
Crystal size (nm)*	700 × 600
Instrument	TEM Philips CM120
Reflections: measured, unique, observed [$I > 3\sigma(I)$]	4855, 424, 283
R_{int}	0.384
$(\sin\theta/\lambda)_{max}$ (Å^{-1})	0.708
$R[I > 3\sigma(I)]$, $wR(F)$, S	0.244, 0.260, 8.77
No. of reflections	424
No. of parameters	11

*Third dimension not known.

hakite crystal were consistent with the cubic Laue group $m\bar{3}m$ and systematic absences for an *I*-centred cell. The structure was refined in space group $I\bar{4}3m$, in accordance with other members of the tetrahedrite group. The chosen space group was confirmed by analysis of electron density found by *Superflip* (Palatinus and van der Lee, 2008). Details of data collection and structure refinement are given in Table 6. Final refined atom coordinates and displacement parameters are given in Table 7.

Description of the crystal structure

The structure of hakite is demonstrably isotypic with the tetrahedrite structure. The structure may be described as stacking of layers of Se-centred polyhedra. A regular planar network of the corner-sharing $SeCu_3Sb$ tetrahedra, all oriented with the apical atom on one side of the layer, is modified either by a vacant tetrahedral site or by replacing three tetrahedra by one $SeCu_6$ octahedron. The layers are stacked along (111) so that an octahedron in one layer is placed below the vacant tetrahedral site of the other layer, and the apical atoms of one layer become the basal atoms of the adjacent layer. Mercury atoms are most likely to occupy the Cu1 position, which has much larger average distances (2.56 Å) to the nearest Se atoms than the Cu2 position (2.14 Å). The refinement is consistent with this assumption, yielding the occupancy of Hg in the Cu1 site of ~20%, while the occupancy of Hg in the Cu2 site refines very close to zero. The refinement result corresponds to 1.21 Hg apfu. Given the limited accuracy of the refinement from the electron-diffraction data, this result is in good agreement with the results of the chemical analysis of the sample studied, 1.54 Hg apfu (n = 4). The refinement did not indicate the presence of S at the two non-equivalent Se sites, but detection of a small amount of S in these sites is probably beyond the accuracy of the current data.

Discussion and conclusions

Hakite is one of the relatively common microscopic selenides in the Příbram uranium and base-metal district. Tetrahedrite and chalcopyrite often occur on the border of the calcite veins containing selenides and uraninite, but they are probably later than the Se mineralization. The evolution of hydrothermal fluids, from which selenide minerals formed, shows a distinct enrichment in sulfur and depletion in selenium with time. For the case of berzelianite, which is one of the most common

TABLE 7. Refined atom parameters for Hg-hakite.

Atom	Wyckoff site	*x/a*	*y/b*	*z/c*	U_{iso}/Å^2	Occ.
Sb1	8*c*	0.2349	0.2349	0.2349	0.004	1
Se1	2*a*	0	0	0	0.059	1
Se2	24*g*	0.3998	0.3998	0.1506	0.037	1
Cu1	12*d*	0.25	0.5	0	0.008	0.797
Hg1	12*d*	0.25	0.5	0	0.008	0.203
Cu2	12*e*	0.1970	0	0	0.032	1

https://doi.org/10.1180/minmag.2016.080.038 Published online by Cambridge University Press

macroscopic minerals in Příbram associated with hakite, the lowest temperature of formation is 113°C. Below this temperature berzelianite is expected to decompose into umangite, Cu_3Se_2 (Chakrabarti and Laughlin, 1981). As umangite was observed only rarely in the direct association with hakite, we infer that mineral associations containing hakite formed in most cases at temperatures above 113°C. This inference was not precluded by temperatures of homogenization of inclusions (Žák and Dobeš, 1991), which showed temperatures of formation of the carbonate veins with uraninite in Příbram in the range 80–140°C. While the hakites at Příbram are mostly Hg-dominant (i.e. hakite *sensu stricto*), more rarely Zn-dominant and Cd-dominant, and tetrahedrite is either Zn- or Fe-dominant. Coupling of Hg with Zn is manifested in Figs 7 and 8. Good miscibility of Hg and Zn and poor miscibility of Hg and Fe was described for synthetic tetrahedrites by Karup-Møller and Makovicky (2004). Also, preferential miscibility of Cd with Zn is clear. There are no mineral markers containing Fe, Zn, Cd or Hg tied to the Fe-, Zn-, Cd- or Hg-hakite types in most cases. Tiemannite is relatively frequent in the selenide assemblage but Hg-hakite is not limited to the tiemannite association. Minerals containing Zn and Fe are very rare in the association; only cadmoselite occurs in close association with Cd-hakite.

According to a study of so-called Se-tetrahedrites, Karup-Møller and Makovicky (1999) found that in the case of the complete substitution of Se for S, only the fully substituted, (Zn, Fe for Cu substitution) $Cu_{10}(Zn,Fe)_2Sb_4Se_{13}$ tetrahedrites exist, unlike under-substituted compositions that are unstable. A few unpublished experiments undertaken by the above-mentioned authors suggested that with an increasing sulfur content this limitation is relaxed and the progressively more and more under-substituted varieties may occur as well. Figure 9 shows that in general all hakites are (nearly) fully substituted, so that the hakite occurrence is in full agreement with this finding for synthetic material.

Hakite from Příbram concentrates Hg, Cd and Ag, while tetrahedrite concentrates Fe, Zn and Cu. This phenomenon may be caused by a larger ionic radius of selenium atoms with respect to sulfur. Selenides contain larger voids in the structure, which may more easily host larger cations such as Hg, Ag or Cd. Another reason could be a change in fluid chemistry over the time of crystallization (tetrahedrite is younger than hakite). The As-dominant analogue of hakite, giraudite (Johan *et al.*, 1982), has been found in the Příbram district only extremely rarely. One of the reasons is the

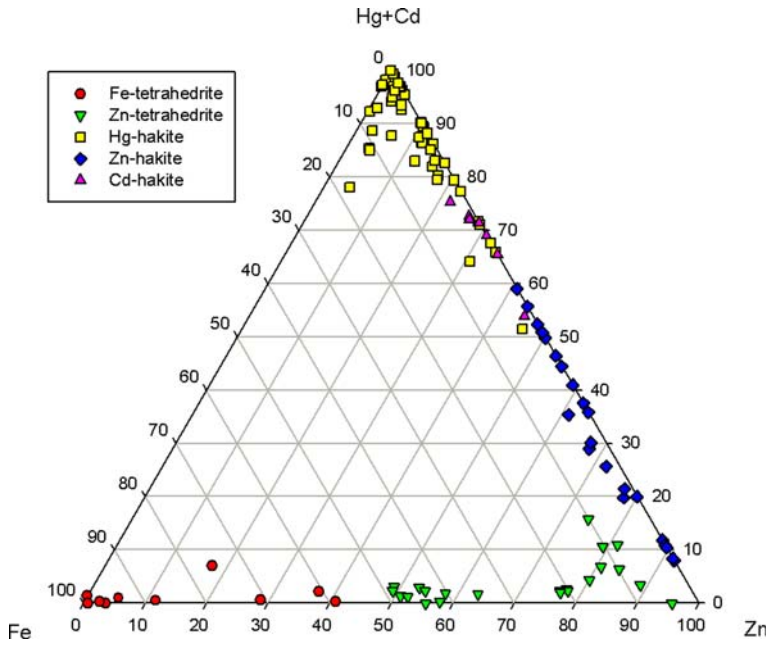


FIG. 7. Ternary plot of Hg+Cd, Fe, Zn contents in tetrahedrite-group minerals from Příbram.

https://doi.org/10.1180/minmag.2016.080.038 Published online by Cambridge University Press

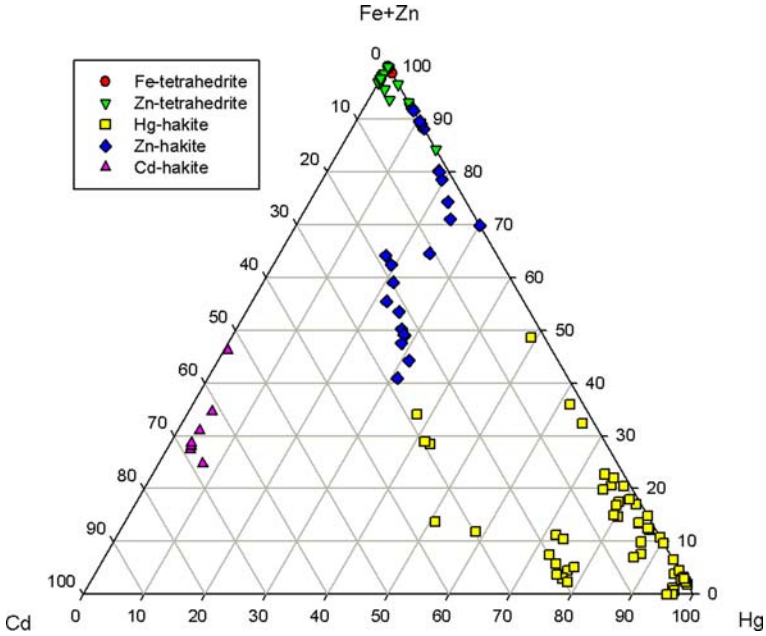


FIG. 8. Ternary plot of Fe+Zn, Hg, Cd contents in tetrahedrite-group minerals from Příbram.

overall predominance of Sb over As in the later hydrothermal fluids occurring both in the Příbram–Březové Hory base-metal and the Příbram uranium and base-metal districts (Škácha *et al.*, 2012). Presence of the two As modifications and löllingite also indicate the possibility that the fugacities of Se and S were too low to oxidize arsenic to As^{3+}. The rare association of luzonite and tennantite shows that at least locally the fugacity of sulfur was sufficient to oxidize arsenic to As^{3+} or As^{5+} later in the mineralization process.

In general, Hg minerals are very rare at Příbram, with the exception of the Hg-rich silver (from other parts of the district), Hg-hakite and tiemannite (HgSe), which are locally abundant. Cinnabar is rare in the whole uranium and base-metal Příbram

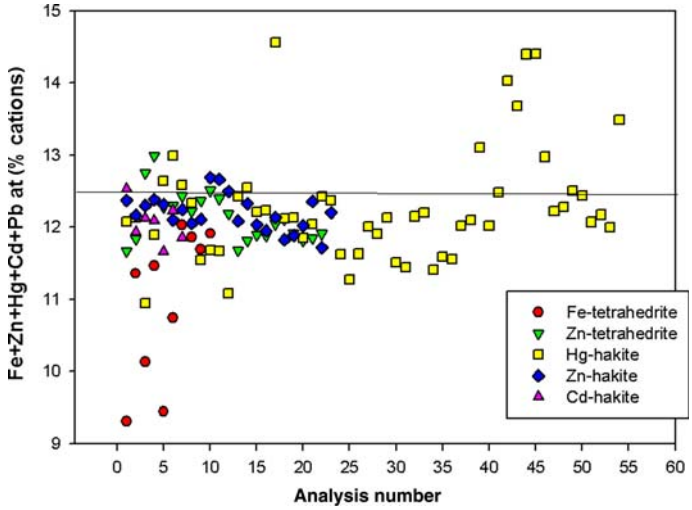


FIG. 9. Plot of Fe+Zn+Hg+Cd+Pb at.% of all cations *vs.* analysis number of tetrahedrite-group minerals from Příbram.

https://doi.org/10.1180/minmag.2016.080.038 Published online by Cambridge University Press

district. The Se-bearing association most probably originated from As–Se bearing fluids at the beginning of the Se-mineralization stage, depositing native arsenic with small clausthalite inclusions, arsenolamprite and small aggregates of berzelianite. Crystallization of arsenic and arsenolamprite (As) under the above conditions led to a decrease of the As/Sb activity ratio, resulting in only small amounts of As left available for the main mineralizing phase. The later mineral assemblage, which contains most of the selenides including hakite, formed under conditions of high a_{Se_2}/a_{S_2} ratios. However, minor parts of this dominant selenide mineralization were leached out during subsequent hydrothermal processes, leading to the latest suite of selenium minerals, such as idiomorphic antimonselite and the selenium analogue of chalcostibite (Škácha *et al.*, 2015). Crystallization of the Sb- and Se-dominant minerals continued until a decrease in the activity of selenium and antimony, and an increase of the sulfur fugacity in the fluids occurred, which led to the crystallization of tetrahedrite and chalcopyrite. At least at the beginning of this process, Fe-Zn-, Zn-Fe- and Zn-tetrahedrites with elevated selenium contents crystallized and even reversals in solution chemistry occurred occasionally, as indicated in Fig. 2.

High oxidation potentials of fluids is demonstrated by the occurrence of otherwise rare under-substituted Se-rich Fe-tetrahedrite, according to the nomenclature of Makovicky and Karup-Møller (1994), as shown in Fig. 4, where the dominating Fe-tetrahedrite trend deviates from the rest of the tetrahedrites. Most tetrahedrite-group members follow the 1:1 to 2:0 mixing-line for Me^{2+} (in Fig. 4), except for the Se-rich Fe-tetrahedrite, which follows a line from the $1Fe{:}1Me^{2+}$ ratio to the $1.5Fe{:}0Me^{2+}$ ratio. At the former end of the line, $2Fe^{2+}$ apfu are obviously occupying the *C* position in the formula of Fe-tetrahedrite. At the latter end, however, the *C* position is occupied by $1Fe^{2+} + 1/2Fe^{3+} + 1/2Cu^{+}$ in this case. Therefore, Se-rich Fe-tetrahedrite from the Příbram selenide occurrence is a rare, under-substituted Fe-tetrahedrite, very probably because of the high oxidation potential of the mineralizing solutions, which favoured preservation of Fe^{3+} in the phase. The selenide minerals in the Příbram district formed within the stability field of hematite, between 5.8 and 7 log units f_{O_2}. This high $f_{O_2(g)}$ condition enhances the separation of selenium from sulfur, leading to a high f_{Se_2}/f_{S_2} ratio and to deposition of a diverse group of selenides. The actual mineralogy and the amount of selenide minerals that form from such oxidizing fluids is a function of f_{Se_2} and ultimately reflect the concentration of selenium in the fluids (Simon *et al.*, 1997).

Acknowledgements

We are indebted to František Laufek (Czech Geological Society) for his kind consultations on the hakite structure. The helpful comments of an anonymous reviewer, as well as Associate Editor Mark Welch, are greatly appreciated. The research was financially supported by project GA14–27006S of the Czech Science Foundation for PŠ and JS and by the Institutional Research Plan No. AV010100521 of the Institute of Physics ASCR, v.v.i. for JP and LP.

References

Anderson, E.B. (1987) *Isotopic-geochronological investigation of the uranium mineralization of Czechoslovakia.* Unpublished Czechoslovak Uranium Industry Report 1962-87.

Brodin, B.V. (1981) Silver-bearing hakite. *International Geology Review*, **23**, 71–73.

Burnham, C.W. (1962) Lattice constant refinement. *Carnegie Institute of Washington Yearbook*, **61**, 132–135.

Chakrabarti, D.J. and Laughlin, D.E. (1981) The Cu–Se (copper-selenium) system. *Bulletin of Alloy Phase Diagrams*, **2**, 305–315.

Dymkov, J.M. (1985) Selenidy nasturan-karbonatnych žil. Pp. 153–162 in: *Paragenezis mineralov uranonosnych žil.* Nedra, Moscow.

Förster, H.-J., Rhede, D. and Tischendorf, G. (2002) Continuous solid solution between mercurian giraudite and hakite. *The Canadian Mineralogist*, **40**, 1161–1170.

Förster, H.-J. and Rhede, D. (2004) Mineralogy of the Niederschlema – Alberoda U-Se-polymetallic deposit, Erzgebirge, Germany. III. First indication for complete miscibility between tennantite and giraudite. *The Canadian Mineralogist*, **42**, 1719–1732.

Hatert, F. and Burke, E.A.J. (2008) The IMA–CNMNC dominant-constituent rule revisited and extended. *The Canadian Mineralogist*, **46**, 717–728.

Johan, Z. and Kvaček M. (1971) La hakite, un nouveau minéral du groupe de la tetraédrite. *Bulletin de la Société française de minéralogie et de cristallographie*, **94**, 381–384.

Johan, Z., Picot, P. and Ruhlmann, F. (1982) Evolution paragénétique de la minéralisation uranifère de Chaméane (Puy-de-Dôme), France: chaméanite, geffroyite et giraudite, trois séléniures nouveaux de Cu, Fe, Ag et As. *Tschermaks Mineralogische und Petrographische Mitteilungen*, **29**, 151–167.

Karup-Møller, S. and Makovicky, E. (1999) Exploratory studies of the solubility of minor elements in tetrahedrite. Part II. Selenium and tellurium as

https://doi.org/10.1180/minmag.2016.080.038 Published online by Cambridge University Press

anions in Zn-Fe tetrahedrites. *Neues Jahrbuch für Mineralogie, Monatshefte*, 385–399.

Karup-Møller, S. and Makovicky, E. (2003) Exploratory studies of the solubility of minor elements in tetrahedrite. Part V. Mercurian tetrahedrite. *Neues Jahrbuch für Mineralogie, Monatshefte*, 73–83.

Karup-Møller, S. and Makovicky, E. (2004) Exploratory studies of the solubility of minor elements in tetrahedrite VI. Zinc and the combined zinc-mercury substitutions. *Neues Jahrbuch für Mineralogie, Monatshefte*, 508–524.

Kolb, U., Gorelik, T., Kuebel, C., Otten, M.T. and Hubert, D. (2007) Towards automated diffraction tomography: Part I – Data acquisition. *Ultramicroscopy*, **107**, 507–513.

Kopecký, S., Pauliš, P. and Škoda R. (2010) Nový nález selenidů na výskytu uranových rud Černý Důl v Krkonoších (Česká republika). *Bulletin mineralogicko – petrologického oddělení Národního Muzea*, **18**(2), 43–49.

Kvaček, M. (1973) Selenides from the uranium deposits of western Moravia, Czechoslovakia – part 1. *Acta Universitatis Carolinae: Geologica*, **1–2**, 23–36.

Kvaček, M. (1979) Selenides from the uranium deposits of western Moravia, Czechoslovakia – part 2. *Acta Universitatis Carolinae: Geologica*, **1–2**, 15–38.

Kvaček, M. (1987) Mineralogicko – geochemická charakteristika selenidového zrudnění na uranových ložiskách Českého masivu. Pp. 89–95 in: *Mineralogia uránových a s nimi súvisiacích nerastných surovín.* Sborník Spišská Nová Ves, Slovenia.

Litochleb, J., Šrein, V., Novická, Z. and Šreinová B. (1999) Selenidy z uranového ložiska Ústaleč (jz. *Čechy). Bulletin mineralogicko – petrologického oddělení Národního Muzea*, **7**, 98–108.

Makovicky, E. and Karup-Møller, S. (1994) Exploratory studies on substitution of minor elements on sythetic tetrahedrite. Part I. Substitution by Fe, Zn, Co, Ni, Mn, Cr, Vand Pb. Unit-cell parameter changes on substitution and the structural role of "Cu^{2+}". *Neues Jahrbuch für Mineralogie, Abhandlungen*, **167**, 89–123.

Moëlo, Y., Makovicky, E., Mozgova, N.N., Jambor, J.J., Cook, N., Pring, A., Paar, W., Nickel, E.H., Graeser, S., Karup-Møller, S., Balic-Žunic, T., Mumme, W.G., Vurro, F., Topa, D., Bindi, L., Bente, K. and Shimizu, M. (2008) *Suphosalts systematics: a review.* Report of the suphosalt sub-comittee of the IMA Commission on Ore Mineralogy. *European Journal of Mineralogy*, **20**, 7–46.

Ondruš, P. (1995) *ZDS – software for analysis of X-ray powder diffraction patterns. Version 6.01. User's Guide.* Prague.

Paar, W.H., Topa, D., Roberts, A.C., Criddle, A.J., Amann, G. and Sureda, R.J. (2002) The new mineral species brodtkorbite, Cu_2HgSe_2, and the associated selenide assemblage from Tuminico, Sierra de Cacho, La Rioja, Argentina. *The Canadian Mineralogist*, **40**, 225–237.

Palatinus, L. (2011) *PETS – program for analysis of electron diffraction data.* Institute of Physics of the ASCR, Prague.

Palatinus, L. and Chapuis, G. (2007) Superflip – a computer program for the solution of crystal structures by charge flipping in arbitrary dimensions. *Journal of Applied Crystallography*, **40**, 451–456.

Palatinus, L. and van der Lee, A. (2008) Symmetry determination following structure solution in P1. *Journal of Applied Crystallography,* **41,** 975–984

Petříček, V., Dušek M. and Palatinus, L. (2014) Crystallographic Computing System JANA2006: General features. *Zeitschrift für Kristallographie*, **229**, 345–352.

Pouchou, J.L. and Pichoir, F. (1985) "PAP" (φρZ) procedure for improved quantitative microanalysis. Pp. 104–106 in: *Microbeam Analysis* (J.T. Armstrong, editor). San Francisco Press, San Francisco.

Scharmová, M. and Scharm, B. (1995) Minerály selenu na uranovém ložisku Zadní Chodov. *Bulletin mineralogicko – petrologického oddělení Národního Muzea*, **3**, 43–47.

Sejkora, J., Macek, I., Škácha, P., Pauliš, P., Plášil, J. and Toegel, V. (2014) Výskyt asociace Hg a Tl selenidů na opuštěném uranovém ložisku Zálesí v Rychlebských horách (Česká republika). *Bulletin mineralogicko – petrologického oddělení Národního Muzea*, **22**, 333–345.

Shannon, R.D. (1981) Bond distances in sulphides and a preliminary table of sulphide crystal radii. *Structure and Bonding in Crystals*, **2**, 53–70.

Simon, G., Kesler, S.E. and Essene, E.J. (1997) Phase relations among selenides, suphides, tellurides, and oxides: II. Applications to selenide-bearing ore deposits. *Economic Geology*, **92**, 468–484.

Škácha, P., Sejkora, J., Knížek, F., Slepička, V., Litochleb, J. and Jebavá, I. (2012) Výskyty unikátního monometalického stříbrného zrudnění na žíle H14F3 mezi 7. a 9. patrem šachty č. 21 Háje, příbramský uran-polymetalický revír (Česká republika): *Bulletin mineralogicko-petrologického oddělení*, **20**, 230–254.

Škácha, P., Plášil, J., Sejkora, J. and Goliáš, V. (2015) Suphur-rich antimonselite, $Sb_2(Se,S)_3$ in the Se-bearing mineral association from the uranium and base metal ore district Příbram, Czech Republic. *Journal of Geosciences*, **60**, 23–29.

Yvon, K., Jeitschko, W. and Parthé, E. (1977) Lazy Pulverix, a computer program for calculation X-ray and neutron diffraction powder patterns. *Journal of Applied Crystalography*, **10**, 73–74.

Žák, K. and Dobeš, P. (1991) Stable isotopes and fluid inclusions in hydrothermal deposits: the Příbram ore region. *Rozpravy Československé akademie věd, Řada Matematických a Přírodních Věd*, **101**, 1–109.

https://doi.org/10.1180/minmag.2016.080.038 Published online by Cambridge University Press